Original Research Article

Stability of Cracked Functionally Graded Graphene-Reinforced Beams under Magnetic Field

ABSTRACT

This paper investigates dynamic stability of cracked functionally graded (FG) graphene platelet (GPL)-reinforced composite laminated beams within the framework of the first-order shear deformation theory. The cracked beam is subjected to the combined action of a periodic axial force and magnetic field. GPL weight fraction follows a layer-wise variation across the beam thickness. Effective material properties are estimated by micromechanics models, and the bending stiffness of the cracked section is evaluated by a massless rotational spring model. The governing equation is derived by Ritz method and Lagrange equation, and the unstable regions of the cracked beams are determined by Bolotin method. Numerical results show that magnetic field intensity, GPL distribution pattern, crack depth and location have significant influence on the dynamic stability behaviors of the cracked beams.

Keywords: Crack; Functionally graded materials; Graphene platelet; The first-order shear deformation theory; Dynamic stability

1. INTRODUCTION

Traditional composites are prone to stress concentration at the interface of different components because of the mismatch of physical properties, which often lead to delamination or cracks when the structure is subjected to large mechanical or temperature load. In the cutting-edge scientific and technological fields such as aviation, ships, engines and so on, materials are often required to work normally in extreme environments such as ultra-high pressure, ultra-high / low temperature, etc. [1]. Relying on traditional composites can no longer meet the strict requirements of structural performance in these fields. With the rapid development of material science, polymer nanocomposites, as the most promising direction of composites, now occupy an important position in the development strategy of new materials all over the world.

Adding a small amount of GPLs to the polymer matrix can significantly

improve the mechanical, thermal and electrical properties of the composites [2-4]. Compared with carbon nanotubes, GPLs have better reinforcement properties for matrix mechanical parameters [2]. The reasonable functional gradient distribution of multiphase materials can reduce or even eliminate the interface damage caused by different properties of different materials. Most recently, Yang and his co-workers [5-7] introduced the concept of FG multilayer materials into GPL-reinforced composites. Through systematic research, it is found that the reasonable distribution of graphene in the matrix can further increase the natural frequencies and static critical buckling loads of the structures, and reduce the forced vibration response of the structures. Kitipornchai et al. [8] studied the buckling behavior of FG GPL-reinforced composite (FG-GPLRC) porous beams. The results show that the critical buckling loads of porous beams can be effectively increased when both GPL dispersion and porosity distribution pattern are non-uniform and symmetric. Li et al. [9] studied the static buckling of FG-GPLRC porous plates based on an isogeomertic analysis. Lei et al. [10] investigated the buckling behavior of FG-GPLRC laminated plates in thermal environment based on first-order shear deformation theory and meshless kp-Ritz method.

Different from static buckling, when the structure is subjected to dynamic load, a small amplitude of force may lead to structural instability [11]. Therefore, it is very important for the structure to work safely and stably to study the stability behavior of the structure under dynamic load. Wu et al. [12] studied the dynamic instability behavior of FG-GPLRC beams in thermal environment by differential quadrature method. It is found that the distribution of more GPLs near the surface of the beams can effectively increase the natural frequencies of the structures and reduce the width of the instability regions. With the development of science and technology, electromagnetic structures are common in high-tech devices, such as micro / nano devices, high-speed maglev trains and so on. The electromagnetic environment will affect the reliability and safety of elastomer operation. GPL-reinforced composites have a wide range of engineering applications because of their excellent mechanical properties, and the analysis of their structural behavior under magnetic field is an unavoidable topic. Sobhy [13] analyzed the buckling and vibration of FG GPL-reinforced aluminum sandwich curved beams exposed to a magnetic field. Zhang et al. [14] studied the natural frequencies and static buckling of FG-GPLRC cylindrical shells under axial magnetic field, and found that magnetic field has a significant effect on the structural behavior of FG-GPLRC cylindrical shells.

The above studies on FG-GPLRC structures are based on the ideal situation without cracks, but the initial defects in the materials or the damage caused by fatigue or impact can not be avoided completely. It is of great significance to understand the influence of cracks on structural behavior and damage detection. Recently, Song et al. [15] found that when GPLs adopt different distribution

patterns, the natural frequencies and critical buckling loads of FG-GPLRC beams will be affected by cracks in different ways. To the authors' best knowledge, effects of crack defects on the dynamic instability behavior of FG-GPLRC beams under magnetic field have not been reported.

In this paper, the dynamic instability of cracked FG-GPLRC beams under the combined action of periodic axial force and magnetic field is studied. Based on the first-order shear deformation beam theory, the energy function of cracked beams is established. The motion control equation is derived by Ritz method and Lagrange equation, and the principle unstable regions of the beams are determined by Bolotin method. The numerical results of the dynamic instability characteristics of cracked FG-GPLRC beams are given to investigate the effects of cracks on the principle unstable regions of different system parameters.

2. PROBLEM FORMULATION

Fig. 1(a) is a schematic diagram of a cracked FG-GPLRC laminated beam. The beam is perfectly combined by N_L layers of equal thickness, with a total thickness of h and a length of L. The distance between the crack and the left end of the beam is L_1. GPLs are randomly and uniformly dispersed in each layer of the beam, so each layer can be treated as an isotropic uniform material, and the concentration gradually changes with the layer to form a FG structure. According to the distribution pattern of GPLs in the beam, the three cases (UD, FG-O and FG-X) shown in Fig. 1(b) are considered in this paper. GPL volume fraction in each layer is found in Ref. [12], that is, GPLs are concentrated near the neutral layer of FG-O beam and near the top and bottom surface of FG-X beam, but uniformly distributed in UD beam.

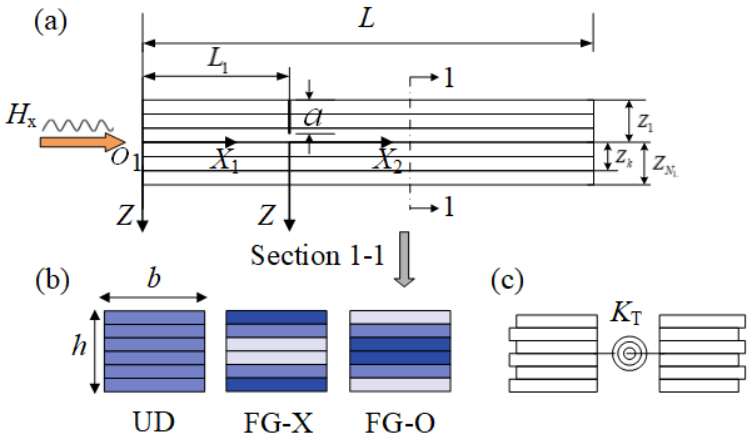

Fig.1 (a) An edge-cracked FG-GPLRC beam; (b) three GPL distribution patterns; (c) the massless rotational spring model

Taking the rectangular GPL stacked by multilayer graphene as an example. According to the modified Halpin-Tsai model and mixing rule [5], the effective Young's modulus E_C, Poisson's ratio ν_C, density ρ_C and magnetic permeability η_C [16] can be approximately obtained.

$$E_{\mathrm{C}}=\frac{3}{8}\frac{1+\xi_{\mathrm{L}}\eta_{\mathrm{L}}V_{\mathrm{G}}}{1-\eta_{\mathrm{L}}V_{\mathrm{G}}}\times E_{\mathrm{M}}+\frac{5}{8}\frac{1+\xi_{\mathrm{W}}\eta_{\mathrm{W}}V_{\mathrm{G}}}{1-\eta_{\mathrm{W}}V_{\mathrm{G}}}\times E_{\mathrm{M}} \tag{1a}$$

$$\nu_{\mathrm{C}}=\nu_{\mathrm{G}}V_{\mathrm{G}}+\nu_{\mathrm{M}}\left(1-V_{\mathrm{G}}\right) \tag{1b}$$

$$\rho_{\mathrm{C}}=\rho_{\mathrm{G}}V_{\mathrm{G}}+\rho_{\mathrm{M}}\left(1-V_{\mathrm{G}}\right) \tag{1c}$$

$$\eta_{\mathrm{C}}=\eta_{\mathrm{G}}V_{\mathrm{G}}+\eta_{\mathrm{M}}\left(1-V_{\mathrm{G}}\right) \tag{1d}$$

where

$$\eta_{\mathrm{L}}=\frac{\left(E_{\mathrm{G}}/E_{\mathrm{M}}\right)-1}{\left(E_{\mathrm{G}}/E_{\mathrm{M}}\right)+\xi_{\mathrm{L}}},\ \eta_{\mathrm{W}}=\frac{\left(E_{\mathrm{G}}/E_{\mathrm{M}}\right)-1}{\left(E_{\mathrm{G}}/E_{\mathrm{M}}\right)+\xi_{\mathrm{W}}} \tag{2}$$

in which the subscripts "*G*" and "*M*" correspond to GPL and matrix material respectively; V_{G} is GPL volume fraction of each layer; $\xi_{\mathrm{L}}=2(l_{\mathrm{G}}/h_{\mathrm{G}})$ and $\xi_{\mathrm{W}}=2(b_{\mathrm{G}}/h_{\mathrm{G}})$ are related to GPL geometry and size, where l_{G}, b_{G} and h_{G} are the average length, width and thickness of GPLs, respectively.

2.1. Rotational spring model

In this paper, the open edge crack perpendicular to the surface of the beam is considered. The massless rotational spring model is used to model cracked FG-GPLRC laminated beam (see Fig. 1(c)), and its effectiveness and accuracy have been verified [15]. According to the theory of fracture mechanics, the flexibility *G* caused by the crack is related to the stress intensity factor at the crack tip.

$$\frac{1-\nu(a)^2}{E(a)}K_{\mathrm{I}}^2=\frac{M^2}{2}\frac{\mathrm{d}G}{\mathrm{d}a} \tag{3}$$

in which *M* is the bending moment of the cross-section of the crack; K_{I} is the stress intensity factor of mode I crack tip under bending load [15]; $E(a)$ and $\nu(a)$ are Young's modulus and Poisson's ratio at the crack tip, respectively. If the normalized stress intensity factor $F(a)=K_{\mathrm{I}}h^2/(6M\sqrt{\pi a})$ is introduced, the following can be obtained from Eq. (3):

$$G=\frac{72\pi}{h^2}\int_0^{\xi}\frac{1-\nu(\varsigma h)^2}{E(\varsigma h)}\varsigma F^2(\varsigma)\mathrm{d}\varsigma \tag{4}$$

where $\varsigma=a/h$. According to the rotational spring model, the stiffness of the rotational spring is:

$$K_{\mathrm{T}}=\frac{1}{G} \tag{5}$$

2.2. Strain energy and potential energy

According to the first-order shear deformation beam theory, the displacements of any point in segment *m* (*m* = 1, 2) along the *X* and *Z* directions are as follows:

$$\begin{aligned}\bar{U}_m(x,z,t) &= U_m(x,t) + z\psi_m(x,t),\\ \bar{W}_m(x,z,t) &= W_m(x,t)\end{aligned} \tag{6}$$

in which $U_m(x,t)$ and $W_m(x,t)$ are the longitudinal and transverse displacements of a point at the neutral plane, respectively; $\psi_m(x,t)$ is the angular displacement of the cross-section; t is time. The strain-displacement relationship is:

$$\varepsilon_{xm} = \frac{\partial U_m}{\partial x} + z\frac{\partial \psi_m}{\partial x},\ \ \gamma_{xzm} = \frac{\partial W_m}{\partial x} + \psi_m \tag{7}$$

then the kinetic energy K and potential energy V of the beam can be expressed as:

$$K = \frac{1}{2}\sum_{m=1}^{2}\int_{L_{0m}}^{L_{1m}}\int_{-h/2}^{h/2}\rho_C\left[\left(\frac{\partial \bar{U}_m}{\partial t}\right)^2 + \left(\frac{\partial W_m}{\partial t}\right)^2\right]\mathrm{d}z\mathrm{d}x \tag{8a}$$

$$\begin{aligned}V = &\frac{1}{2}\sum_{m=1}^{2}\int_{L_{0m}}^{L_{1m}}\int_{-h/2}^{h/2}\left(Q_{11}\varepsilon_{xm}^2 + Q_{55}\gamma_{xzm}^2\right)\mathrm{d}z\mathrm{d}x\\ &+\frac{1}{2}K_{\mathrm{T}}\left[\psi_2(L_1) - \psi_1(L_1)\right]^2\end{aligned} \tag{8b}$$

Define the stiffness components and the inertia-related terms:

$$\left\{A_{11}, B_{11}, D_{11}\right\} = \int_{-h/2}^{h/2} Q_{11}\left\{1, z, z^2\right\}\mathrm{d}z \tag{9a}$$

$$A_{55} = \int_{-h/2}^{h/2}\kappa Q_{55}\mathrm{d}z \tag{9b}$$

$$\left\{I_1, I_2, I_3\right\} = \int_{-h/2}^{h/2}\rho_C\left\{1, z, z^2\right\}\mathrm{d}z \tag{9c}$$

where $\kappa = 5/6$ is shear correction factor; $Q_{11} = E_C/(1-\nu_C^2)$; $Q_{55} = E_C/2(1+\nu_C)$. It is worth noting that the three distribution patterns considered in this paper are all about neutral layer symmetry. From Eqs. (9a) and (9c), it is known that both B_{11} and I_2 are zero, that is, there is no bending-tension coupling effect.

2.3. Maxwell's relation

Ignoring the Thompson effect, the Maxwell electrodynamic equations in elastic media are [17]:

$$\mathbf{J} = \nabla\times\mathbf{h} \tag{10a}$$

$$\nabla\times\mathbf{e} = -\eta_{\mathrm{C}}\frac{\partial \mathbf{h}}{\partial t} \tag{10b}$$

$$\nabla\cdot\mathbf{h} = 0 \tag{10c}$$

$$\mathbf{e} = -\eta_{\mathrm{C}}\left(\frac{\partial \mathbf{U}}{\partial t}\times\mathbf{H}\right) \tag{10d}$$

where **J** is current density; **h** and **e** are the distribution of the induced magnetic field and the intensity of the induced electric field caused by the motion of the

beam, respectively; $\nabla = (\partial / \partial x)\mathbf{i} + (\partial / \partial y)\mathbf{j} + (\partial / \partial z)\mathbf{k}$ is the Hamilton operator; $\mathbf{U} = \bar{U}_m\ \mathbf{i} + 0\ \mathbf{j} + \bar{W}_m\ \mathbf{k}$ is the displacement field of the beam; $\mathbf{i}$, $\mathbf{j}$ and $\mathbf{k}$ are the unit vectors of the *X*, *Y* and *Z* axes, respectively. **H** is the magnetic field distribution in the free space. Eqs (10b) and (10d) can derive:

$$\mathbf{h} = \nabla \times \left(\mathbf{U} \times \mathbf{H} \right) \tag{11}$$

Considering the axial magnetic field, i.e., $\mathbf{H} = H_x \mathbf{i}$, and substituting Eq. (6) into Eq. (11), yields

$$\mathbf{h} = -H_x \frac{\partial \bar{W}_m}{\partial z} \mathbf{i} + H_x \frac{\partial \bar{W}_m}{\partial x} \mathbf{k} \tag{12}$$

then the Lorentz force generated by the axial magnetic field is:

$$f_m = \eta_{\mathrm{C}} (\mathbf{J} \times \mathbf{H}) = \eta_{\mathrm{C}} \left(0\mathbf{i} + 0\mathbf{j} + H_x^2 \frac{\partial^2 \bar{W}_m}{\partial x^2} \mathbf{k} \right) \tag{13}$$

It can be seen from Eq. (13) that when the specific case is considered in this paper, only the component $f_z = \eta_{\mathrm{C}} H_x^2 \dfrac{\partial^2 W_m}{\partial x^2}$ in the Z direction of f_m is left, and the Lorentz force is a function of permeability and H_x. The ideal graphene is intrinsically non-magnetic and lacks localized magnetic moment because of a delocalized π-bonding network. Therefore, the discussion in this paper assumes that the permeability η_{G} of GPLs is zero [18], then according to Eqs. (6) and (13), the Lorentz magnetic force are:

$$\begin{aligned} F_{lm} &= \int_{-h/2}^{h/2} f_z dz = H_x^2 \frac{\partial^2 W_m}{\partial x^2} \int_{-h/2}^{h/2} \eta_{\mathrm{C}} dz \\ &= H_x^2 \frac{\partial^2 W_m}{\partial x^2} \int_{-h/2}^{h/2} \eta_{\mathrm{M}} \left(1 - V_{\mathrm{G}}\right) dz = \eta_{\mathrm{M}} h \left(1 - V_{\mathrm{G}}^*\right) H_x^2 \frac{\partial^2 W_m}{\partial x^2} \end{aligned} \tag{14}$$

where V_{G}^* is the total GPL volume fraction, which is related to total GPL weight fraction g_{G}:

$$V_{\mathrm{G}}^* = \frac{g_{\mathrm{G}}}{g_{\mathrm{G}} + (\rho_{\mathrm{G}} / \rho_{\mathrm{M}})(1 - g_{\mathrm{G}})} \tag{15}$$

The external work done by axial excitation $N_{\mathrm{x}0}$ and magnetic force is as follows:

$$\Upsilon_{\mathrm{p}} = \frac{1}{2} \sum_{m=1}^{2} \int_{L_{0m}}^{L_{1m}} \left[N_{\mathrm{x}0} \left(\frac{\partial W_m}{\partial x} \right)^2 + F_{lm} W_m \right] \mathrm{d}x \tag{16}$$

3. SOLUTION PROCEDURE

3.1. Ritz trial functions

The convergence of the solution can be promoted by selecting the potential function which satisfies both the geometric boundary conditions and the compatibility conditions between the beam segments at the crack. Therefore, this paper first makes the potential functions of the two beam segments satisfy their own geometric boundary conditions respectively, and then modifies the potential function of segment 1 to make the compatibility conditions set up. Introducing the following dimensionless quantities:

$$\begin{gathered}
\zeta_1=\frac{x}{L},\quad \zeta_2=\frac{x-L_1}{L-L_1},\quad (u,w)=\frac{(U,W)}{h},\varphi=\psi,\\
\alpha=\frac{L_1}{h},\quad \alpha_1=\frac{L-L_1}{h},\quad \tau=t\sqrt{\frac{A_{11}}{I_1L_1(L-L_1)}},\\
\left(\bar{I}_3,d_{11},a_{55}\right)=\left(\frac{I_3}{I_1h^2},\frac{D_{11}}{A_{11}h^2},\frac{A_{55}}{A_{11}}\right),\quad \beta=\frac{L-L_1}{L_1},\\
k_{\mathrm{T}}=\frac{L-L_1}{A_{11}h^2}K_{\mathrm{T}},\quad P=\frac{N_{x0}}{A_{11}},\quad H_x^*=\frac{\eta_{\mathrm{M}}hH_x^2}{A_{11}}
\end{gathered}\tag{17}$$

then the compatibility conditions of the beam at the crack are as follows:

$$\begin{gathered}
u_1(1)=u_2(0),\quad w_1(1)=w_2(0),\\
k_T[\varphi_2(0)-\varphi_1(1)]=d_{11}\frac{\partial\varphi_2(0)}{\partial\zeta_2}
\end{gathered}\tag{18}$$

Considering clamped-clamped support at both ends, the potential function of the beam can be selected:

$$\begin{gathered}
u_1=\sum_{j=1}^{N}A_j\zeta_1^j(1-\zeta_1)+\zeta_1\sum_{j=1}^{N}a_j,\quad u_2=\sum_{j=1}^{N}a_j(1-\zeta_2)^j,\\
w_1=\sum_{j=1}^{N}B_j\zeta_1^j(1-\zeta_1)+\zeta_1\sum_{j=1}^{N}b_j,\quad w_2=\sum_{j=1}^{N}b_j(1-\zeta_2)^j,\\
\varphi_1=\sum_{j=1}^{N}C_j\zeta_1^j(1-\zeta_1)+\zeta_1\sum_{j=1}^{N}c_j\left(1+\frac{jd_{11}}{k_{\mathrm{T}}}\right),\\
\varphi_2=\sum_{j=1}^{N}c_j(1-\zeta_2)^j
\end{gathered}\tag{19}$$

3.2. Dynamic instability analysis

Substituting Eqs. (8) and (16) into the second kind of Lagrange equation:

$$\frac{\mathrm{d}}{\mathrm{d}\tau}\left(\frac{\partial\Pi}{\partial\dot{d}_l}\right)-\frac{\partial\Pi}{\partial d_l}=Q_l,\quad l=1,2,...,6N \tag{20}$$

where $\Pi=K-V$ is Lagrangian function, $Q_l=\partial\Upsilon_{\mathrm{p}}/\partial d_l$ is generalized force, and d_l is an unknown coefficient A_j, B_j, C_j, a_j, b_j or c_j. Furthermore,

considering Eq. (17), the dimensionless motion equations of cracked beam can be obtained, and the matrix form is

$$\mathbf{M}\ddot{\mathbf{d}}+\left(\mathbf{K}_{\mathrm{L}}-\mathbf{K}_{\mathrm{H}}-P\,\mathbf{K}_{\mathrm{P}}\right)\mathbf{d}=\mathbf{0} \tag{21}$$

where $\mathbf{d}=\left\{\{A_j\}^{\mathrm{T}}\ \{a_j\}^{\mathrm{T}}\ \{B_j\}^{\mathrm{T}}\ \{b_j\}^{\mathrm{T}}\ \{C_j\}^{\mathrm{T}}\ \{c_j\}^{\mathrm{T}}\right\}^{\mathrm{T}}$, $\mathbf{M}$ is the mass matrix, $\mathbf{K}_{\mathrm{L}}$ is the stiffness matrix, $\mathbf{K}_{\mathrm{H}}$ and $\mathbf{K}_{\mathrm{P}}$ are the geometric stiffness matrix. This paper considers the case of axial periodic load, i.e.,

$$P=P_{\mathrm{s}}+P_{\mathrm{d}}\cos\theta\tau \tag{22}$$

in which P_{s} and P_{d} represent static and dynamic components, respectively.

Expanding the displacement vector **d** in the following series:

$$\mathbf{d}=\sum_{\mathrm{n}=1,3,\ldots}^{\infty}\boldsymbol{\alpha}_{\mathrm{n}}\sin\left(\frac{n\theta\tau}{2}\right)+\boldsymbol{\beta}_{\mathrm{n}}\cos\left(\frac{n\theta\tau}{2}\right) \tag{23}$$

where $\boldsymbol{\alpha}_{\mathrm{n}}$ and $\boldsymbol{\beta}_{\mathrm{n}}$ are arbitrary constant vectors. The Bolotin method [19] shows that the first-order approximation of Eq. (23) can provide good accuracy for calculating the boundary of the unstable region. By substituting Eqs. (22) and (23) into Eq. (21), two independent eigenvalue equations are obtained:

$$\left[\mathbf{K}_{\mathrm{L}}-\mathbf{K}_{\mathrm{H}}-\left(P_{\mathrm{s}}-\frac{P_{\mathrm{d}}}{2}\right)\mathbf{K}_{\mathrm{P}}-\frac{\theta^2}{4}\mathbf{M}\right]\boldsymbol{\alpha}_1=0 \tag{24a}$$

$$\left[\mathbf{K}_{\mathrm{L}}-\mathbf{K}_{\mathrm{H}}-\left(P_{\mathrm{s}}+\frac{P_{\mathrm{d}}}{2}\right)\mathbf{K}_{\mathrm{P}}-\frac{\theta^2}{4}\mathbf{M}\right]\boldsymbol{\beta}_1=0 \tag{24b}$$

When P_{d} takes a specific value, two critical excitation frequencies θ can be found as eigenvalues. The region surrounded by the relation curve between θ and P_{d} is the principle unstable region of the beam.

4. NUMERICAL RESULTS AND DISCUSSION

4.1. Comparison studies

In this section, through an example, the results calculated by this method are compared with those in the literature to verify the accuracy of this method. Tables 1 and 2 show the dimensionless fundamental frequencies and critical buckling loads of craked functionally graded material (FGM) beams clamped at both ends without magnetic field, respectively. Beam thickness h = 0.1 m and crack depth ratio is 0.2. The Young's modulus and density of the beams follow the variation law of exponential function along the thickness direction, that is, $E(Z)=E_0\exp(\beta Z)$, $\rho(Z)=\rho_0\exp(\beta Z)$, and Poisson's ratio remains constant 0.33. The elastic modulus and density of the material on the top surface of cracked beams are $E_1=70\,\mathrm{GPa}$ and $\rho_1=2780\,\mathrm{kg/m^3}$, respectively. Table 1 is the result when the crack is at the midspan of the beam, while Table 2 is the result

when the Young's modulus ratio of the bottom surface to the top surface of the beam is $E_2 / E_1 = 5$ and the slenderness ratio of the beam is 6. It can be seen that the error between the results of this paper and those of Ref. [20] is very small.

Table 1 Dimensionless fundamental frequencies of cracked FGM beams.

E_2/E_1	L/h=6			L/h=16		
	Present	Ref. [20]	Error	Present	Ref. [20]	Error
0.2	0.8197	0.8125	0.89%	0.3600	0.3602	0.04%
1.0	0.8688	0.8584	1.21%	0.3848	0.3840	0.20%
5.0	0.8416	0.8289	1.52%	0.3653	0.3641	0.33%

Table 2 Dimensionless critical buckling loads of cracked FGM beams.

	L_1/L						
	0.1	0.2	0.3	0.4	0.5	0.6	0.7
Ref [20]	0.1487	0.1544	0.1552	0.1510	0.1484	0.1510	0.155 2
Present	0.1494	0.1544	0.1544	0.1487	0.1457	0.1487	0.1544
Error	0.47%	0.00%	0.52%	1.52%	1.82%	1.52%	0.52%

4.2. Parametric studies

In the following example, cracked FG-GPLRC beams with a thickness of 0.12 m and slenderness ratio of 10 are considered, and the total number of layers of the beams is 10. Each layer is uniformly mixed with epoxy resin and GPLs, in which the average dimensions of GPLs are $l_G = 2.5\,\mu\text{m}$, $w_G = 1.5\,\mu\text{m}$ and $h_G = 1.5\,\text{nm}$, respectively. The material parameters of GPL and epoxy resin can be found in Ref. [15].

Fig. 2 studies the effect of GPL distribution pattern on the principle unstable regions of cracked FG-GPLRC beams under magnetic field. It can be seen that with the same depth and location of cracks, the FG-X beams have the highest resonance frequencies, while the FG-O beams have the lowest resonance frequencies. Compared with the UD beam, the principle unstable region of the FG-X beam moves to the direction of the increase of the excitation frequency, while the principle unstable region of the FG-O beam moves to the direction of the decrease of the excitation frequency. This is because the distribution of GPLs far away from the neutral layer has a better strengthening effect on the structure. The results also show that the enhancement of the magnetic field has a significant effect on improving the dynamic stability of the beams, increasing the resonance frequencies and reducing the width of the principle unstable regions. At the same time, it can be seen that when the magnetic field intensity increases from 0 to 0.2, the displacement of the principle unstable region of the FG-O beam is the largest in the direction of the increase of the excitation frequency, while that of the FG-X beam is the smallest. Therefore, the change of magnetic field has the greatest effect on the principle unstable regions of cracked FG-O beams and the least

effect on the principle unstable regions of cracked FG-X beams.

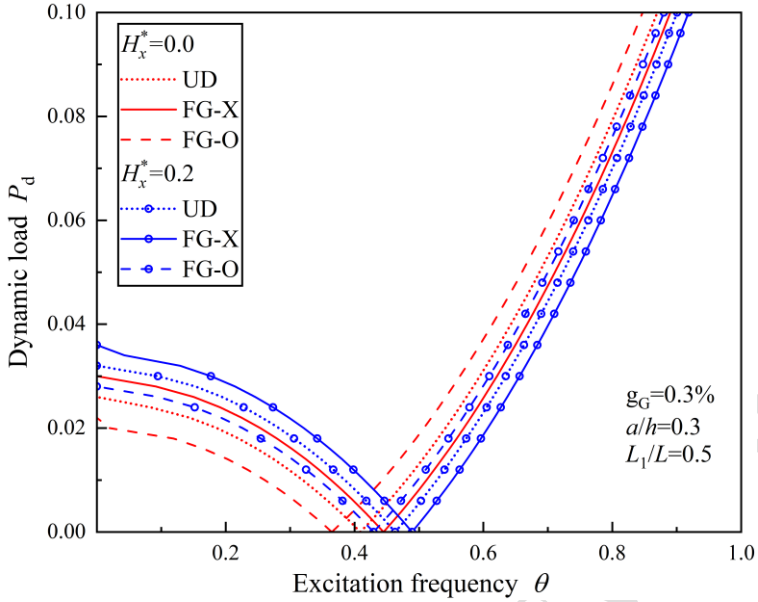

Fig. 2. Effect of GPL distribution pattern on the principle unstable regions of cracked beams

Fig. 3 investigates the effect of crack depth on the principle unstable regions of FG-GPLRC beams under the action of magnetic field. Four cases in which the crack depth ratio is 0.0, 0.1, 0.2 and 0.3 are taken into account in the calculation, in which the crack depth ratio of 0.0 means that the beam does not contain crack. It can be seen from the figure that with the increase of the crack depth, the principle unstable region of the beam moves to the direction of the decrease of the excitation frequency, and the width of the principle unstable region increases, that is, the increase of crack depth will reduce the dynamic stability of the beam. Moreover, it can be further observed that the width of the principle unstable region increases faster with the increase of crack depth.

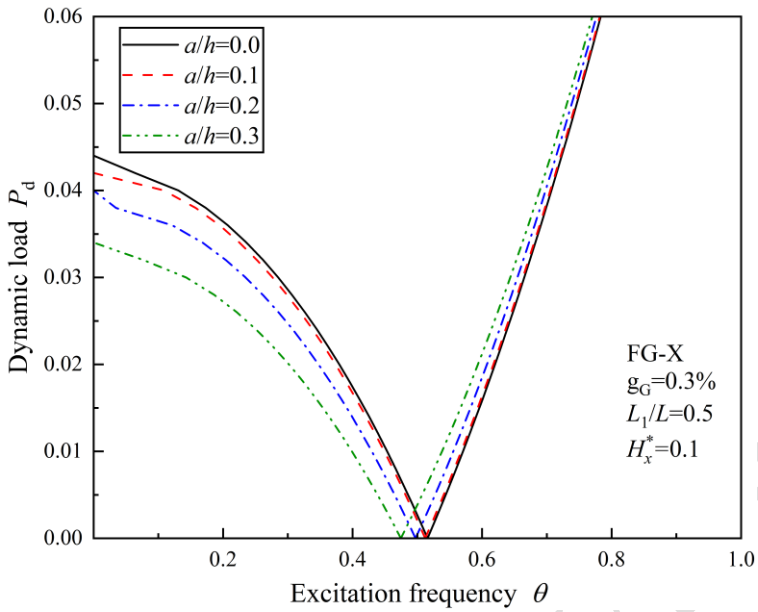

Fig. 3. Effect of crack depth on the principle unstable regions of cracked beams

Fig. 4 illustrates the effect of crack location on the principle unstable regions of FG-GPLRC beams under the action of magnetic field. When the crack location moves from one end to the midspan of the beam, the width of the principle unstable region of the beam becomes larger, and the resonance frequency also increases. Further observation shows that when the crack is near one end of the beam, the change of its location has a great effect on the resonance frequency, while when the crack is near the midspan, its location has a weak effect on the resonance frequency.

Fig. 5 presents the effect of magnetic field intensity on the principle unstable regions of FG-GPLRC beams. It can be seen that with the enhancement of the magnetic field, the principle unstable region of the cracked beam first moves to the direction of the increase of the excitation frequency, until the intensity of the magnetic field reaches about 0.3, and then to the direction of the decrease of the excitation frequency. This is because the magnetic field force is transverse along the beam, and its magnitude is related to the transverse displacement of the beam, so that the enhancement of the magnetic field promotes the instability of the beam on the one hand, and improves the stiffness of the beam on the other hand. When the magnetic field is weak, the effect of increasing stiffness is greater than that of promoting instability on the dynamic stability of the beams, while when the magnetic field is strong, the effect of promoting instability is greater.

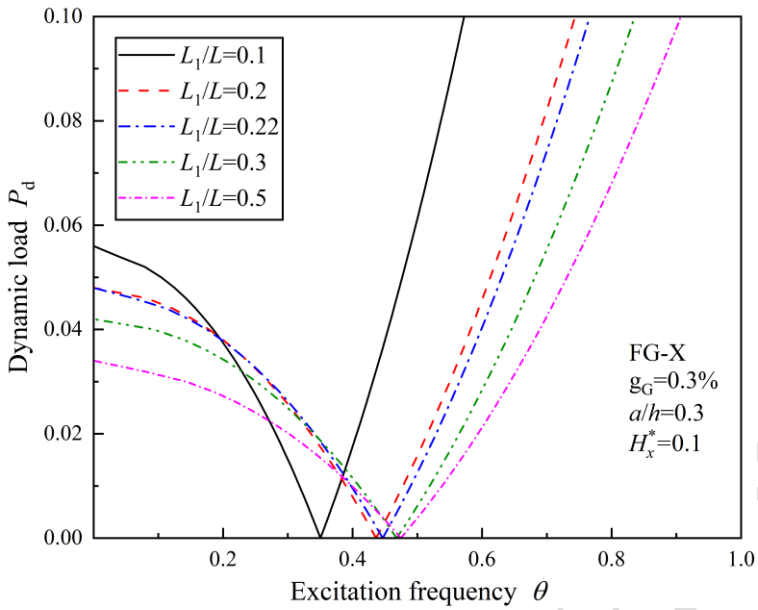

Fig. 4. Effect of crack location on the principle unstable regions of cracked beams

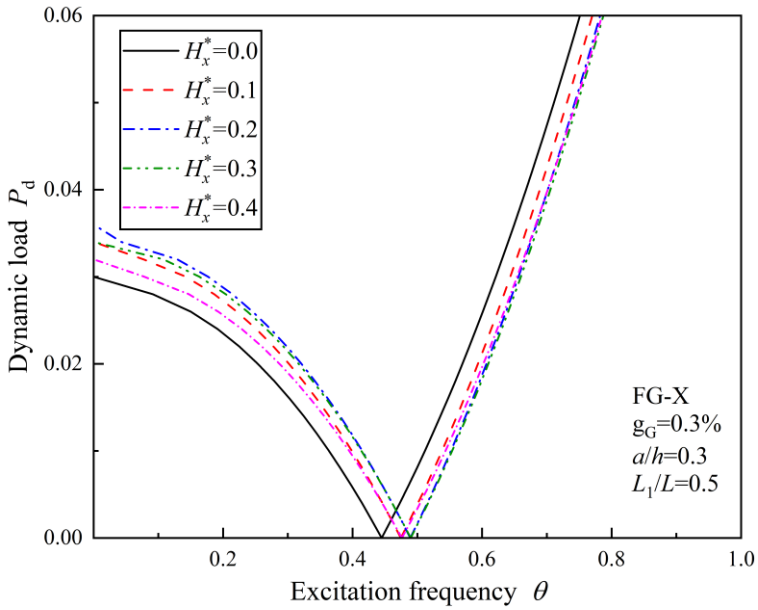

Fig. 5. Effect of magnetic field intensity on the principle unstable regions of cracked beams

5. CONCLUSIONS

Based on the first-order shear deformation beam theory and the massless rotational spring model, the dynamic instability of cracked FG-GPLRC beams under axial load in magnetic field is studied in this paper. The mechanical parameters of GPL-reinforced composites were estimated by micromechanical model and mixing rule. The principle unstable regions of cracked FG-GPLRC beams were calculated by combining Ritz method, Lagrange equation and

Bolotin method. The numerical results show that: (1) The dynamic stability of cracked beams can be improved by properly strengthening the magnetic field. The excessive magnetic field will reduce the dynamic stability of the beams. (2) With the same depth and location of cracks, the principle unstable regions of FX-O beams are the most sensitive to the change of magnetic field intensity, while the principle unstable regions of FG-X beams are the least sensitive to magnetic field. (3) The existence of cracks can reduce the resonance frequencies of the beams and increase the width of the principle unstable regions. The effect is related to the crack location and increases with the increase of the crack depth.

REFERENCES

[1] Qin Z, Wu YT, Eizad A, Lyu SK, Lee CM. Advancement of Mechanical Engineering in Extreme Environments. International Journal of Precision Engineering and Manufacturing-Green Technology. 2021;8(6):1767-82.

[2] Rafiee MA, Rafiee J, Wang Z, Song HH, Yu ZZ, Koratkar N. Enhanced Mechanical Properties of Nanocomposites at Low Graphene Content. Acs Nano. 2009;3(12):3884-90.

[3] Mortazavi B, Benzerara O, Meyer H, Bardon J, Ahzi S. Combined molecular dynamics-finite element multiscale modeling of thermal conduction in graphene epoxy nanocomposites. Carbon. 2013;60:356-65.

[4] Wang Y, Yu JH, Dai W, Song YZ, Wang D, Zeng LM, et al. Enhanced Thermal and Electrical Properties of Epoxy Composites Reinforced With Graphene Nanoplatelets. Polymer Composites. 2015;36(3):556-65.

[5] Song MT, Kitipornchai S, Yang J. Free and forced vibrations of functionally graded polymer composite plates reinforced with graphene nanoplatelets. Composite Structures. 2017;159:579-88.

[6] Yang J, Wu HL, Kitipornchai S. Buckling and postbuckling of functionally graded multilayer graphene platelet-reinforced composite beams. Composite Structures. 2017;161:111-8.

[7] Chen D, Yang J, Kitipornchai S. Nonlinear vibration and postbuckling of functionally graded graphene reinforced porous nanocomposite beams. Composites Science and Technology. 2017;142:235-45.

[8] Kitipornchai S, Chen D, Yang J. Free vibration and elastic buckling of functionally graded porous beams reinforced by graphene platelets. Materials & Design. 2017;116:656-65.

[9] Li KY, Wu D, Chen XJ, Cheng J, Liu ZY, Gao W, et al. Isogeometric Analysis of functionally graded porous plates reinforced by graphene platelets. Composite Structures. 2018;204:114-30.

[10] Lei ZX, Su QQ, Zeng HP, Zhang Y, Yu CH. Parametric studies on buckling behavior of functionally graded graphene-reinforced composites laminated plates in thermal environment. Composite Structures. 2018;202:695-709.

[11] Ke LL, Yang J, Kitipornchai S. Dynamic Stability of Functionally Graded Carbon Nanotube-Reinforced Composite Beams. Mechanics of Advanced Materials and Structures. 2013;20(1):28-37.
[12] Wu HL, Yang J, Kitipornchai S. Dynamic instability of functionally graded multilayer graphene nanocomposite beams in thermal environment. Composite Structures. 2017;162:244-54.
[13] Sobhy M. Buckling and vibration of FG graphene platelets/aluminum sandwich curved nanobeams considering the thickness stretching effect and exposed to a magnetic field. Results in Physics. 2020;16:102865.
[14] Zhang CW, Wang LM, Eyvazian A, Khan A, Sebaey TA. Analytical solution for static and dynamic analysis of FGP cylinders integrated with FG-GPLs patches exposed to longitudinal magnetic field. Engineering with Computers. (*in press*).
[15] Song MT, Gong YH, Yang J, Zhu WD, Kitipornchai S. Free vibration and buckling analyses of edge-cracked functionally graded multilayer graphene nanoplatelet-reinforced composite beams resting on an elastic foundation. Journal of Sound and Vibration. 2019;458:89-108.
[16] Liu DY. Free Vibration of Functionally Graded Graphene Platelets Reinforced Magnetic Nanocomposite Beams Resting on Elastic Foundation. Nanomaterials. 2020;10(11):2193.
[17] Rad AB, Shariyat M. Three-dimensional magneto-elastic analysis of asymmetric variable thickness porous FGM circular plates with non-uniform tractions and Kerr elastic foundations. Composite Structures. 2015;125:558-74.
[18] Orlita M, Escoffier W, Plochocka P, Raquet B, Zeitler U. Graphene in high magnetic fields. Comptes Rendus Physique. 2013;14(1):78-93.
[19] Bolotin VVe. The Dynamic Stability of Elastic Systems. American Journal of Physics. 1965;33(9):752-3.
[20] Ke LL, Yang J, Kitipornchai S, Xiang Y. Flexural Vibration and Elastic Buckling of a Cracked Timoshenko Beam Made of Functionally Graded Materials. Mechanics of Advanced Materials and Structures. 2009;16(6):488-502.